Chinese Chemical Letters 34 (2023) 107996

Contents lists available at ScienceDirect

Chinese Chemical Letters

journal homepage: www.elsevier.com/locate/cclet

MXene fibers for electronic textiles: Progress and perspectives

Jianmin Li[a,*], Chaoyang Miao[a], Jing Bian[a], Shayan Seyedin[b,*], Ke Li[c,*]

[a] *College of Electronic and Optical Engineering & College of Flexible Electronics (Future Technology), Nanjing University of Posts and Telecommunications, Nanjing 210023, China*

[b] *School of Engineering, Newcastle University, Newcastle upon Tyne NE1 7RU, United Kingdom*

[c] *Centre for Research on Adaptive Nanostructures and Nanodevices (CRANN) & Advanced Materials and BioEngineering Research (AMBER) Centre, School of Chemistry, Trinity College Dublin, Dublin, Dublin 2, Ireland*

ARTICLE INFO

Article history:
Received 27 September 2022
Revised 10 October 2022
Accepted 7 November 2022
Available online 9 November 2022

Keywords:
MXene
Liquid crystal
Wet spinning
Conductive fiber
Functional textile
Flexible electronics

ABSTRACT

The rapid evolution of portable and wearable electronic devices has fueled the development of smart functional textiles that are able to conduct electricity, sense body movements, or store energy. One main challenge inhibiting the further development of functional textile-based electronics is the lack of robust functional fibers with suitable electrical, electrochemical and sensing functionalities. MXenes, an emerging family of two-dimensional (2D) materials, have shown to be promising candidates for producing functional fibers due to their exceptional electrical and electrochemical properties combined with solution processability. The unique ability of MXenes to readily form liquid crystal phases in various solvents has allowed them to generate additive-free fibers using a wet spinning process. In this work, we review the recent exciting developments in the fabrication of neat MXenes fibers and present a critical evaluation of practical challenges in MXenes processing that influence the macroscale material properties and the performance of the subsequent devices. We also provide our assessment for the future opportunities and challenges in producing MXene fibers to help pave the way for their widespread use in advanced wearable applications.

1. Introduction

Small electronic devices incorporated into gadgets that can be worn on the human body (*i.e.*, wearable smart watches) are now widely used for entertainment, communication, fitness tracking, and health monitoring. In the near future, a new generation of wearable gadgets is expected to be developed by using soft and breathable electronic textiles (E-textiles) that could be worn in the same way as conventional clothes [1–4]. This will require access to novel functional fibers that offer suitable electrical, electrochemical, electronic, and optoelectronic properties (in addition to the one-dimensional fiber form factor) for use as flexible wires, energy storage or harvesting devices, sensors (*e.g.*, strain, pressure, touch, moisture, gas, or chemical), flexible display devices, and electronic building blocks like transistors [5–18]. The enhanced level of human interaction with technology achieved by employing functional fibers can ultimately lead to improved health, connectivity, and entertainment. The estimated increase in the global smart textiles market from ~\$0.5 billion in 2015 to ~\$9.3 billion by 2024 indicates the growing demand for textile products with new functionalities, suggesting that clothes made using novel functional fibers could soon find their way to the market [19].

A wide range of functional materials such as conducting polymers [20–22], one-dimensional (1D) materials (*e.g.*, carbon nanotubes and gold nanowires) [23–26] and two-dimensional (2D) materials (*e.g.*, graphene, MoS_2, and MXenes) [27–38] have been developed and shown suitable electrical, electronic, and electrochemical properties to achieve functional fibers for wearable applications. MXenes, a rapidly developing family of 2D materials [30,39-41] with an unprecedented combination of high electrical conductivity (up to 15,000 S/cm) [42], excellent electrochemical properties (volumetric capacitance of up to 1,500 F/cm^3) [43], and solution processibility, are increasingly utilized in fiber-based applications. MXenes ($M_{n+1}X_nT_x$) are typically synthesized by removing the “A” layer from the parent MAX ($M_{n+1}AX_n$) phases (“M”, early transition metal; “A”, Group 13-16 elements, “X”, carbon and/or nitrogen, and $n = 1$-4) *via* chemical etching using concentrated hydrofluoric acid or a mixture of lithium fluoride and hydrochloric acid (minimally intensive layer delamination method) or electrochemical etching [30,38-41]. Terminating groups “T” (*e.g.*, =O, –OH and/or –F) introduced during the synthesis process (x is

---

[*] Corresponding authors.

E-mail addresses: lijm@njupt.edu.cn (J. Li), shayan.seyedin@newcastle.ac.uk (S. Seyedin), like@tcd.ie (K. Li).

https://doi.org/10.1016/j.cclet.2022.107996

the number of T groups) provide MXenes with solution processibility, which suits a variety of fabrication routes, such as coating, inkjet printing, solution spinning, and electrospinning to produce MXene-based fibers [10,44-54]. In early reports, $Ti_3C_2T_x$ MXene was used as a coating layer on silver-plated nylon yarns [44] and carbon fibers [45] to produce fiber-based electrodes with an areal capacitance of ~328 mF/cm^2 and length capacitance of ~253 mF/cm, respectively, showing potential in fiber supercapacitor devices. Coating on a commercial fiber or yarn is a facile approach for producing functional fibers and was used to manufacture $Ti_3C_2T_x$ MXene-coated cellulose yarns (*e.g.*, cotton, bamboo and linen) with MXene loading of up to ~77 wt%. The obtained fibers showed an electrical conductivity of up to ~440 S/cm, length capacitance of ~760 mF/cm, excellent washability (45 cycles at temperatures up to 80 °C), and knittability into pressure sensor textiles [51]. Researchers also employed solution spinning approach to produce fibers with high MXene loadings to fully utilize the outstanding properties of MXenes in fiber-based systems. Initially, $Ti_3C_2T_x$ MXene was incorporated into dispersions of graphene oxide (GO) [47,55] or poly(3,4-ethylenedioxythiophene):poly(styrene sulfonate) (PEDOT:PSS) [56] to achieve spinnable formations that could be made into hybrid fibers using solution spinning. This was done because the initial attempts in making neat (additive-free) MXene fibers failed as the result of using MXenes with relatively small lateral sizes (< 1 μm) and the lack of suitable coagulating formulations [47]. Nevertheless, reduced GO (rGO)/$Ti_3C_2T_x$ MXene hybrid fibers with MXene loadings of up to ~95 wt% were produced, which showed a volumetric capacitance of up to ~586 F/cm^3 [47,55]. The recent discovery of nematic liquid crystal (LC) phases in additive-free MXene dispersions such as $Ti_3C_2T_x$ and $Mo_2Ti_2C_3T_x$ opened doors to producing neat MXene fibers [53,57]. This research area has gained considerable momentum in recent years and there have been important achievements in neat MXene fiber processing and applications.

This review provides an overview of the recent progress in the development of neat MXene fibers enabled by the distinctive LC property in MXene dispersions. In this review, we first explain the evolution of the nematic LC phase in MXenes and discuss factors affecting LC properties in MXenes and the rheological implications of the LC formulations as relevant to solution spinning. Then we provide details of the MXene fiber formation process, coagulation mechanisms, and factors that impact the spinnability of MXene dispersions. This is followed by discussions on properties of MXene fibers, which include electrical, mechanical, and electrochemical properties, leading to a diverse range of applications such as fiber-based wires, heaters, and energy storage devices (*e.g.*, supercapacitors). We finally provide an evaluation of the progress achieved in recent years, highlight the challenges presented in the field, and provide directions for future research. We hope the discussions in this review could facilitate the development of fibers that utilize the full potential of MXenes in fiber-based structures, leading to a new generation of MXene fibers that suit a diverse range of wearable applications.

2. Rheological properties of MXenes

The rheological properties of MXene dispersions play a critical role in the spinning process of MXene fiber. The oxygen-rich surface terminations of MXenes flakes endow MXenes with a high negative surface charge, which allows for good dispersibility of MXenes in a wide range of polar solvents [58–60]. For instance, $Ti_3C_2T_x$ MXene can be dispersed in water with very high concentrations exceeding 100 mg/mL [53]. Notably, the negative surface charge of $Ti_3C_2T_x$ MXene is enhanced with increasing the pH value, indicating strong electrostatic repulsion in neutral and basic environments (Fig. 1a). In addition, the high aspect ratio (*i.e.*, width/thickness) of MXenes makes them possible to form nematic LC mesophases in solution [57]. Nematic phases are identified as topological features called disclinations, which are manifested by birefringent optical textures (*i.e.*, schlieren textures) consisting of dark and bright brushes under crossed polarizers. Based on theoretical predictions from the Onsager's model, an isotropic dispersion containing randomly oriented flakes, such as MXene dispersions, may turn into an anisotropic state with long-range orientational ordering and form the nematic phases at a critical transition concentration (C_t) [61]. C_t for the isotropic-nematic (I-N) transition decreases with increasing the MXene flake size (Fig. 1b).

Zhang *et al.* first reported the LC properties in additive-free aqueous dispersions of $Ti_3C_2T_x$ MXene with different flake sizes by observing the evolution of birefringence in $Ti_3C_2T_x$ inks under polarized optical microscopy [53]. As shown in Fig. 1c, the birefringence appeared at ~6.3 mg/mL for the large-size $Ti_3C_2T_x$ (L-$Ti_3C_2T_x$, ~3.1 μm), while a significantly higher concentration of ~58.0 mg/mL was needed for the small-size $Ti_3C_2T_x$ (S-$Ti_3C_2T_x$, ~310 nm) to achieve birefringence. The schlieren textures, that indicate the complete I-N transition, were observed at ~13.2 mg/mL for L-$Ti_3C_2T_x$ and ~66.3 mg/mL for S-$Ti_3C_2T_x$. The LC properties of $Ti_3C_2T_x$ were also observed in polar organic solvents, such as dimethyl sulfoxide (Fig. 1d), *N*-methyl-2-pyrrolidone (Fig. 1e), and *N*,*N*-dimethylformamide (Fig. 1f). However, a higher concentration (~20 mg/mL) was needed for L-$Ti_3C_2T_x$ MXene in these solvents, than in water, to achieve I-N transition, which could be caused by the polarity of the solvent. In other words, it is easier for a solvent with higher polarity to induce the I-N transition in MXene dispersions. In addition, the nematic LC phases were observed in aqueous dispersions of other MXenes such as small-flake $Mo_2Ti_2C_3T_x$ and Ti_2CT_x at a concentration of ~100 mg/mL, which was at the same range as the S-$Ti_3C_2T_x$ [53].

The rheological properties of MXenes are related to their flake size and concentration, in agreement with the behavior shown by other 2D materials like GO [53,62-64]. The L-$Ti_3C_2T_x$ dispersion showed a high zero-shear viscosity of ~5,050 Pa s at ~26.5 mg/mL, while a higher concentration of ~150 mg/mL was needed for S-$Ti_3C_2T_x$ to achieve the same viscosity level [53]. In addition, the elastic modulus (G') was typically higher than the viscous modulus (G'') throughout the frequency range for both large and small flake $Ti_3C_2T_x$ MXene inks at the full nematic phase transition concentrations (Figs. 1g and h). The ratio of G'/G'' of MXene LC dispersion plays an important role during the wet-spinning process of MXene fiber. Generally, a G'/G'' value of over 1, which indicates gel-like properties, is required to ensure spinnability. The high delamination and gelation of MXene dispersions are also essential for continuous fiber preparation.

3. Fabrication of MXene fibers

The shear-thinning non-Newtonian behavior of MXene dispersions enables them to flow continuously throughout a nozzle upon extrusion to form a stable stream of solution called jet, which is the pre-requisite for fiber formation. There are multiple mechanisms for the spinning process of MXene fibers. One popular mechanism is the polyelectrolyte complexation process induced by a positively charged polymer such as chitosan. This mechanism was first reported by Zhang *et al.* for MXene fiber fabrication [53]. Another mechanism for the wet-spinning of MXene fibers relies on the significant colloidal stability destruction of MXene sheets induced by salt ions and/or solvents. This mechanism has been widely used for fabricating MXene hydrogels and aerogels [65,66]. The positively charged ions or polymers in the coagulation, which show strong electrostatic interaction to the negatively charged functional groups of MXene flakes, have the potential to be used as coagulating agents for MXene fiber spinning. The typ-

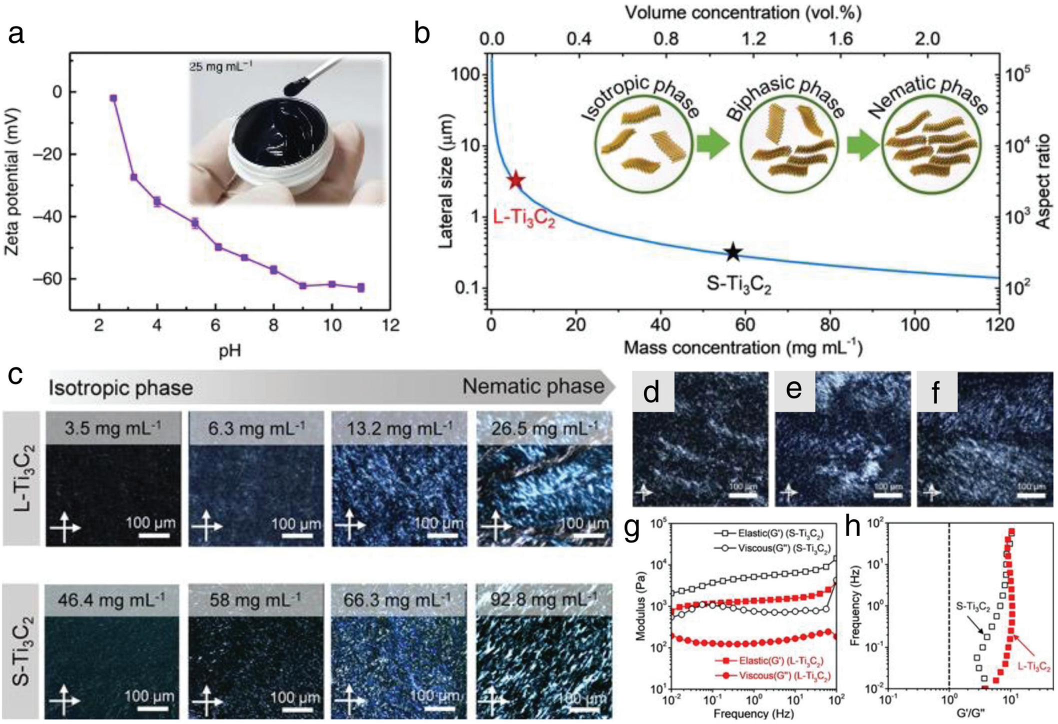

Fig. 1. (a) Zeta potential of $Ti_3C_2T_x$ MXene aqueous dispersion as a function of pH. The inset in (a) is a digital image of a $Ti_3C_2T_x$ MXene dispersion at a concentration of ~25 mg/mL. Reproduced with permission [62]. Copyright 2020, Springer Nature Limited. (b) Relationship between the $Ti_3C_2T_x$ MXene ink concentration and the flake size for isotropic to nematic phase transition based on theoretical calculations. (c) Polarized optical microscopy images of aqueous L-$Ti_3C_2T_x$ and S-$Ti_3C_2T_x$ inks at various concentrations. Polarized optical microscopy images of L-$Ti_3C_2T_x$ in (d) dimethyl sulfoxide, (e) *N*-methyl-2-pyrrolidone, and (f) *N,N*-dimethylformamide. (g) Viscoelastic behavior of L-$Ti_3C_2T_x$ at a concentration of ~26.5 mg/mL and S-$Ti_3C_2T_x$ at a concentration of ~150 mg/mL. (h) Frequency dependence of G'/G'' ratio for the L-$Ti_3C_2T_x$ and S-$Ti_3C_2T_x$ MXene inks. Reproduced with permission [53]. Copyright 2021, American Chemical Society.

ical wet-spinning process of MXene fiber is demonstrated in Fig. 2a. The MXene LC dispersion is extruded into a coagulation solution which induces the gelation of MXene flakes. The gel-like fiber is then transferred to a wash bath to remove the residual coagulation solution. Finally, the MXene fiber is dried and collected on a winder. The washing step may be eliminated depending on the coagulation solution used. Zhang *et al.* produced neat MXene fibers by extruding the MXene LC dispersions into various coagulation baths, such as ethanol, 9 mol/L H_2SO_4, 99% acetic acid, 5 wt% $CaCl_2$ aqueous solution, and 0.5 wt% chitosan solution in acetic acid/water solution [53]. The fibers produced by spinning L-$Ti_3C_2T_x$ and S-$Ti_3C_2T_x$ MXene dispersions using acetic acid and chitosan coagulation baths exhibited good mechanical strengths. However, when ethanol, H_2SO_4, or $CaCl_2$ was used as coagulation bath, MXene fibers were weak and difficult to handle. This work also showed that it was possible to produce $Mo_2Ti_2C_3T_x$ fibers by extruding the LC dispersion into an acetone coagulation bath.

The choice of coagulation bath considerably impacts the solidification process during MXene fiber spinning and further affects the fiber morphology. For instance, because of the smaller size of acetic acid than chitosan, it was easier for acetic acid to replace water in the MXene dispersion compared to chitosan, resulting in a rapid coagulation rate for the acetic acid bath [53]. Consequently, MXene fibers with loosely packed morphology, open pores, and irregular cross-section were obtained when acetic acid was used as the coagulant. On the other hand, chitosan with long polymer chains resulted in a slow coagulation rate, leading to MXene fibers with a packed morphology and regular (*i.e.*, round) cross-section. This study highlighted the importance of choosing suitable coagulation baths to achieve MXene fibers with desirable morphology.

A following work by Eom *et al.* reported a continuous spinning process of $Ti_3C_2T_x$ MXene fibers using a NH_4Cl/NH_4OH mixed aqueous solution as a coagulation bath, in which NH_4^+ ions interacted with MXene flakes to bridge between neighboring MXene flakes *via* electrostatic interactions (Figs. 2a-d) [62]. The use of drawing in the wet-spinning process led to MXene fibers showing tightly packed morphology and high orientation [67]. This is consistent with the shear-induced alignment achieved in conventional polymer fibers and other nanomaterials-based fibers such as carbon nanotubes and graphene fibers. Later, Li *et al.* achieved continuous spinning of $Ti_3C_2T_x$ MXene aerogel fibers in an aqueous coagulation bath containing Ca^{2+} ions (Figs. 2e and f) [66]. In addition, a supercritical CO_2 drying process was used following the wet-spinning process, which led to MXene fibers with high porosity (96.5%-99.3%) and specific surface area (~142 m^2/g). Compared to the typical freeze-drying method which could destroy the MXene network structure induced by the ice crystal growth, the supercritical drying process could maintain the structure of the fiber and retain the high MXene flake alignment while achieving high porosity (Figs. 2g and h) [65,68-70]. Apart from the round-shaped MXene fibers made by using circular nozzles, the shape of MXene fiber could be easily adjusted by using extruding nozzles with different shapes. For instance, highly packed flat $Ti_3C_2T_x$ MXene fibers were fabricated by using a flat-shaped needle and a Mg^{2+} ion containing coagulation bath (Figs. 2i and j). Drawing was also applied to achieve a high alignment of MXene flakes in the fiber.

4. Properties of MXene fibers

During the spinning process, the MXene dispersions are first extruded through a narrow nozzle, which applies a shear force sufficient to induce alignment of the ordered LC MXene domains. This aligned state could be retained during the coagulation and solidification processes. As a result, the MXene flakes show high align-

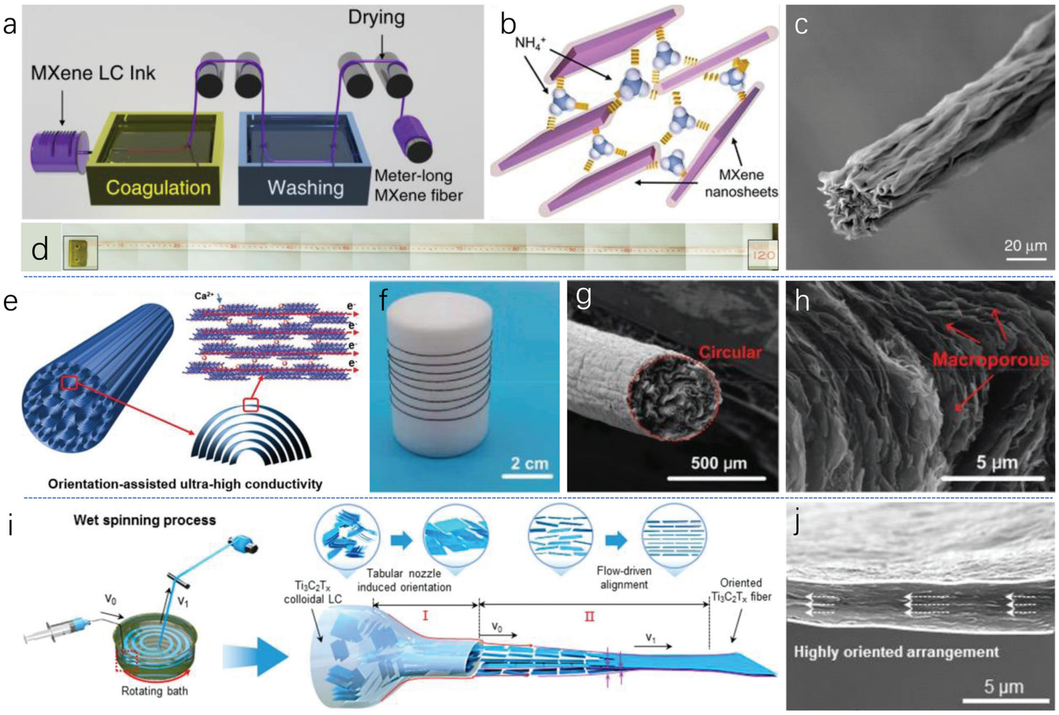

Fig. 2. (a) Schematic illustration of a typical wet-spinning process for producing MXene fibers. (b) Illustration of the mechanism of NH_4^+ ions-MXene flakes interactions. Reproduced with permission [62]. Copyright 2020, Springer Nature Limited. (c) Scanning electron microscopy (SEM) image and (d) digital photograph of a representative $Ti_3C_2T_x$ MXene fiber. Reproduced with permission [67]. Copyright 2021, American Chemical Society. (e) Schematic representation of the fabrication process, (f) digital photograph, and (g, h) SEM images of the orientation-assisted $Ti_3C_2T_x$ MXene aerogel fibers. Reproduced with permission [66]. Copyright 2021, John Wiley & Sons. (i) Schematic illustration of the wet-spinning process, and (j) cross-section SEM image of the flat $Ti_3C_2T_x$ MXene fibers. Reproduced with permission [71]. Copyright 2021, American Chemical Society.

ment along the fiber direction, endowing MXene fibers with good electrical conductivities and mechanical strengths.

The electrical and mechanical properties of MXene fibers are affected by various factors, such as the alignment degree of MXene flakes in the fiber, choice of the coagulation bath, packing morphology, and MXene flake size. L-$Ti_3C_2T_x$ fibers spun in a chitosan bath showed an electrical conductivity of ~7,748 S/cm [53]. While a similar electrical conductivity of ~7,713 S/cm was obtained for $Ti_3C_2T_x$ fibers spun using the NH_4^+ bath; fibers produced in the acetic acid coagulation bath showed a significantly lower conductivity of ~4,048 S/cm [53,67]. S-$Ti_3C_2T_x$ fibers obtained in the chitosan bath only showed a conductivity of ~3,512 S/cm, which was less than half of the electrical conductivity of L-$Ti_3C_2T_x$ fibers (~7,748 S/cm). $Ti_3C_2T_x$ fibers spun from the chitosan bath exhibited a Young's modulus of ~2.3 GPa, a tensile strength of ~40.5 MPa, and an elongation at break of ~1.7%, while fibers spun using the NH_4^+ bath showed a significantly higher Young's modulus of ~29.6 GPa [53,67].

One common approach to enhance the MXene flake alignment in fibers is applying a drawing force during or after fiber spinning. Eom *et al.* applied drawing on the wet MXene fiber in the NH_4^+ coagulation bath using a roller rotating at a rate of 3 times higher than the extrusion rate [67]. As the result, the diameter and the porosity of the $Ti_3C_2T_x$ fiber decreased compared to the undrawn fiber, and the electrical conductivity was enhanced from ~8,260 S/cm to ~12,503 S/cm. Drawing the $Ti_3C_2T_x$ fiber also led to an increase in both the Young's modulus (from ~78.6 GPa to ~122.0 GPa) and the tensile strength (from ~304.4 MPa to ~343.7 MPa), while decreased the elongation at break of the fiber (from ~0.40% to ~0.28%). Li *et al.* used drawing and achieved a flat $Ti_3C_2T_x$ fiber with an enhanced flake alignment, which showed a high conductivity of ~7,200 S/cm, ~2.7 times higher than the fiber produced without drawing (~2,680 S/cm) [71]. The drawn flat fiber exhibited a tensile strength of ~118 MPa, which was significantly higher than the tensile strength of the undrawn fiber (~60 MPa). The drawn fiber also showed a slightly higher elongation at break of ~1.85% compared to the undrawn fiber (elongation at break of ~1.75%).

The drying process was also found to influence the properties of MXene fibers [66]. The natural drying process could cause serious structure collapse induced by the capillary force, while the freeze-induced crystal growth of solvents during the conventional freeze-drying process could destroy the connection between the MXene flakes [72,73]. Li *et al.* introduced a supercritical CO_2 drying technology into the fabrication process of $Ti_3C_2T_x$ MXene fibers, which maintained the porous structure of MXene fibers [66]. The as-prepared fibers showed a highly oriented structure and a high porosity of 96.5%-99.3%, which was much higher than the naturally-dried fibers (porosity <20%). However, the porous $Ti_3C_2T_x$ fiber displayed an electrical conductivity of only ~117.1 S/cm and a tensile strength of ~1.1 MPa with a low elongation at break of 0.35%, because of its high porosity.

Fig. 3 compares the electrical conductivity and Young's modulus of the neat MXene fibers with those of hybrid MXene fibers (*e.g.*, MXene/rGO fiber, MXene/carbon nanotubes fiber, MXene/polyurethane fiber, MXene/polyvinyl alcohol fiber, and MXene/PEDOT:PSS fiber) and graphene fibers produced in the literature [48,49,52,53,55,62,64,66,67,71,74-88]. The electrical and mechanical properties of neat MXene fibers are already on par with or even higher than neat MXene films and are significantly higher than the graphene-based and MXene hybrid fibers. Nevertheless, the mechanical properties of MXene fibers are still significantly lower than those of individual $Ti_3C_2T_x$ flakes (Young's modulus of ~330 GPa and tensile strength of ~17 GPa) [89], suggesting the need to further enhance the interactions between MXene flakes. The properties of MXene fibers fabricated by different methods are summarized in Table 1.

Table 1
The comparison of different fabrication methods of MXene fibers.

Coagulation	Nozzle size (μm)	Nozzle shape	Draw ratio	Flake size (μm)	Fiber diameter (μm)	Density (g/cm^3)	Porosity (%)	Electrical conductivity (S/cm)	Tensile strength (MPa)	Elongation at break (%)	Young's modulus (GPa)	Toughness (MJ/m^3)	Ref.
Acetic acid	130	round	NA	0.31	76.3	1.7	NA	1,942	7.2	0.75	1.0	NA	[53]
				3.1	76.2	1.6	NA	4,048	10.0	1.4	0.7	NA	
	90	round	NA	0.31	34	NA	NA	NA	NA	NA	NA	NA	
				3.1	NA	NA	NA	NA	NA	NA	NA	NA	
Chitosan	130	round	NA	0.31	45.4	3.6	NA	3,512	19.6	1.2	1.6	NA	
				3.1	45.3	3.4	NA	7,750	40.5	1.7	2.4	NA	
	90	round	NA	0.31	33	NA	NA	NA	NA	NA	NA	NA	
				3.1	NA	NA	NA	NA	NA	NA	NA	NA	
NH_4Cl/NH_4OH solution	210	round	NA	2.3	NA	NA	NA	7,713	63.9	0.2	29.6	0.09	[62]
			1.0	4.0	20.3	3.1	21.6	8,259	304.4	0.4	78.6	NA	[67]
			2.0		14.5	3.3	17.2	9,629	316.4	0.3	108.0	NA	
			3.0		11.9	3.7	6.1	1,2503	343.7	0.3	122.0	NA	
0.2 wt% $CaCl_2 \cdot 2H_2O$ solution supercritical CO_2 drying	500	round	NA	5.2	400	0.04	99.3	1,751	1.1	0.3	3	NA	[66]
					400	0.07	98.6	4,617					
					400	0.10	98.1	7,645					
					420	0.20	96.5	11,709					
$MgSO_4$ solution	l = 680	flat	NA	4.3	NA	NA	NA	7,200	118	1.9	6.4	NA	[71]
	w = 210				NA	NA	NA	2,680	60	1.8	3.4	NA	
	510	round			NA	NA	NA	1,260	52	1.2	4.3	NA	

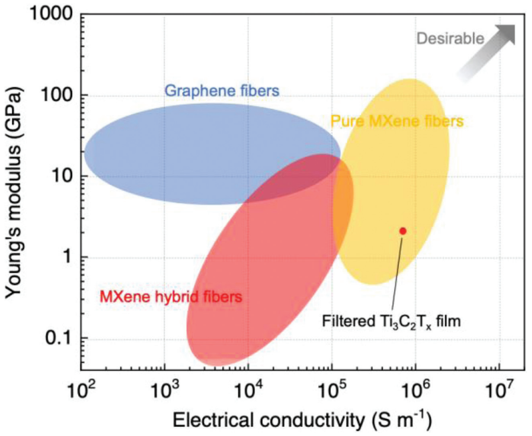

Fig. 3. Comparison of electrical conductivity and Young's modulus of neat MXene fibers with graphene fibers and MXene hybrid fibers [48,49,52,53,55,62,64,66,67,71,74-88].

5. Applications of MXene fibers

The successful spinning of neat MXene fibers is a milestone for building MXene-based macroscale architectures and could hasten the development of high-performance functional E-textiles for future wearable devices. The remarkable electrical and electrochemical properties of neat MXene fibers combined with their flexibility have made them promising candidates for a wide range of applications. One of the most attractive applications is wearable electronics, where the inherent flexibility (Fig. 4a) and strength (Fig. 4b) of MXene fibers could be used in conjunction with their electrical or electrochemical properties. The high electrical conductivity of MXene fibers enabled their use as wires. For instance, Eom *et al.* used MXene fibers as wires in a circuit to turn on a light emitting diode (Fig. 4c) [62]. The MXene fibers were further integrated into a pair of earphones to replace the original metal wire, and the earphones showed a similar sound output to the original ones. Notably, the MXene fibers are lighter than metal wires, enabling the fabrication of devices that are lightweight. This is critical for wearable electronics.

MXene fibers and MXene-coated textiles have also been widely used in electrothermal fields, such as body thermal management and thermal therapy. Zhang *et al.* and Li *et al.* used the neat MXene fibers as Joule heaters and showed that the fiber temperature gradually increased with the input voltage (Fig. 4d) [53,66]. Notably, the MXene fiber exhibited a sensitive thermal response even under an input voltage of only 0.5 V, and its surface temperature reached up to 178°C at an input voltage of 4.5 V, considerably higher than the commercial Toho Tenax carbon fiber heater. Because of the remarkable light-to-heat conversion capability of MXene, induced by its semimetallic localized surface plasmon resonance effect, the MXene aerogel fibers were further used as photothermal fiber, showing a high light responsiveness performance at even low temperatures (Fig. 4e).

MXenes are also very attractive in energy storage applications [90–92]. $Ti_3C_2T_x$ MXene has shown an excellent volumetric capacitance of up to ~1,500 F/cm^3 in supercapacitors, thanks to their superior packing density, metallic conductivity, and fertile redox active sites [43,93]. The S-$Ti_3C_2T_x$ fibers spun in chitosan bath showed a high volumetric capacitance of 1,265 F/cm^3, which was two times higher than that of S-$Ti_3C_2T_x$ fibers spun in an acetic acid bath. This difference in energy storage performance could be attributed to the differences in their packing densities [53]. Li *et al.* also used the oriented flat $Ti_3C_2T_x$ fibers (obtained by drawing) as the electrode materials for supercapacitors, showing a high volumetric capacitance of 1,360 F/cm^3 as well as good rate capability [71]. The same work also assembled the MXene fibers into symmetric fiber-shaped supercapacitors which exhibited good flexibility and wearability when integrated into commercial gloves (Figs. 4f and g).

The results presented above indicate that MXene fibers show comparable properties to MXene films, suggesting their promising potential for the future wearable electronics. However, MXene fiber properties should be further improved to enable their real-life applications in wearable E-textiles. For instance, the mechanical properties of MXene fibers should be enhanced to achieve the tensile strength and stretchability comparable to the traditional clothing fibers such as cotton, polyester, and nylon. The washability, abrasion resistance, and environmental stability of MXene fibers should also be considered for wearable applications.

6. Summary and perspectives

In the past several years, significant progress has been achieved in the exploration of LC phase in MXene dispersions and the production of high-performance MXene fibers using wet-spinning. Recent studies revealed that the interactions between MXene flakes and ions/solvents play a critical role in the spinning process. The neat MXene fibers show excellent electrical and mechanical properties rivaling the graphene-based and MXene hybrid fibers, and present great potential for wearable electronics as conductors, Joule heaters, light heaters, and electrochemical electrodes. However, research in the field of MXene fibers is still in its early stages and there are lots of areas that require further exploration as well as challenges that need to be addressed.

From the perspective of MXene synthesis, optimized strategies that address the scalability and quality of MXene dispersions are highly desirable. The continuous spinning of MXene fibers requires a relatively large amount of MXene dispersions at high concentrations. Also, the chemical etching process usually induces many defects in MXene flakes, which affect the mechanical and electrical properties of the produced MXene fibers. As a result, the efficiency of MXene synthesis needs to improve to yield high-quality and defect-free MXenes.

The LC state of MXene dispersions plays a significant role during the spinning process of MXene fibers. However, the mechanism of the LC formation and factors affecting the LC properties are still not known very well. Notably, the relationship of LC state with size and surface terminations of MXene flakes needs to be explored to tailor the rheological behaviors of MXene dispersions and achieve formulations that are amenable to fiber processing.

The gelation process of MXene dispersions in various solutions should be further studied to shed light on the coagulation mechanism during wet-spinning of MXene fibers. A more detailed understanding of the interactions between MXene flakes and various solvent media and ions is of great importance both in terms of developing novel coagulation mechanisms and enhancing the conductivity and mechanical properties of MXene fibers. Developing a real-time technology to monitor the transition process from the fluid state in the spinning dope to the solid state in the fiber could help control the structure and properties of the MXene fibers.

While methods such as wet-spinning, drop-casting, dip-coating, electrospinning, and biscrolling have been used to achieve MXene-based fibers, so far, only the wet-spinning method has been successfully implemented for the fabrication of neat MXene fibers. Generally, the neat MXene fibers show much higher conductivities compared to the MXene composite or hybrid fibers. However, MXene-based composite or hybrid fibers typically offer higher mechanical properties, such as flexibility and tensile strength. This suggests the needs for more effective fiber fabrication methods to

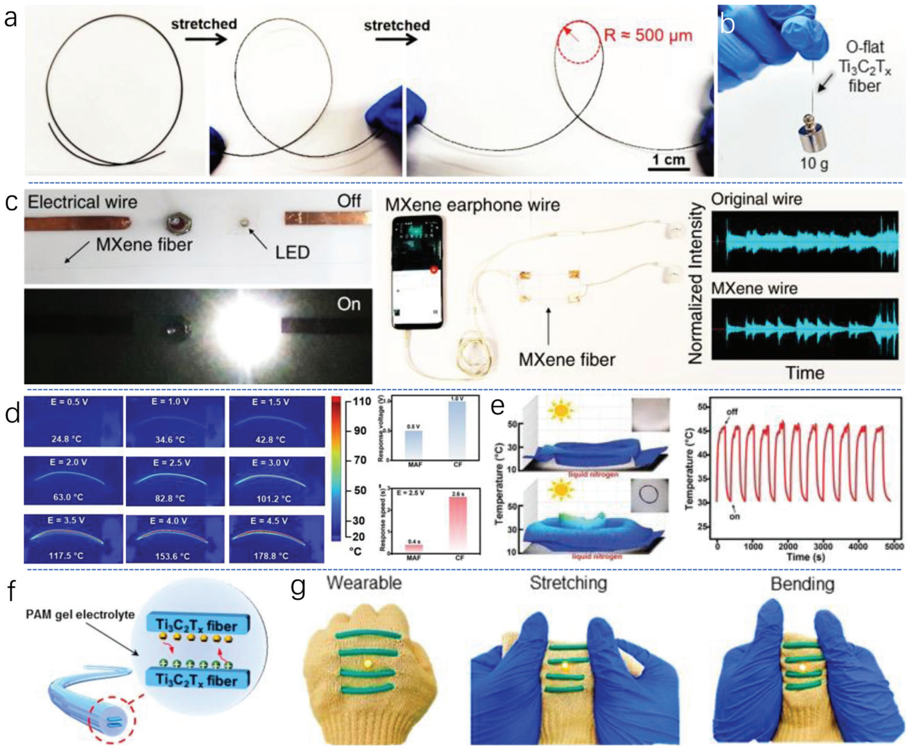

Fig. 4. (a) Flexibility and (b) strength demonstrations of $Ti_3C_2T_x$ MXene aerogel fibers. Reproduced with permission [71]. Copyright 2021, American Chemical Society. (c) $Ti_3C_2T_x$ MXene fibers used as electrical wire and earphone wire. Reproduced with permission [62]. Copyright 2020, Springer Nature Limited. (d) Infrared images of MXene aerogel fiber under different voltages and comparison of the Joule heating performance of MXene aerogel fiber with commercial carbon fiber. (e) 3D infrared photo of MXene aerogel fiber placed on a cold polypropylene surface under solar illumination of 1.0 sun for 2 min and cyclic heating profiles of a bundle of a $Ti_3C_2T_x$ MXene aerogel fiber on a cotton woven fabric under solar illumination of 1.0 sun for ten on/off cycles of light. Reproduced with permission [66]. Copyright 2021, John Wiley & Sons. (f) Schematic illustration and (g) digital photographs of the fiber shaped *quasi*-solid-state supercapacitor integrated into a commercial glove. Reproduced with permission [71]. Copyright 2021, American Chemical Society.

produce neat MXene fibers with both high conductivity and mechanical properties.

The uncontrollable volumetric shrink of MXene fibers during the coagulation and drying processes caused by solvent exchange and/or evaporation could lead to fibers with irregular cross-section morphology, porosity, and wrinkles, which could compromise the mechanical and electrical properties of MXene fibers. Further knowledge of the impact of spinning solvent, MXene dispersion rheology, spinning parameters (*e.g.*, spinneret size and flow rate), and coagulation mechanism could help achieve wrinkle-free MXene fibers with circular cross-section and high structural packing.

Post-stretching after the solidification of MXene dispersions shows to be effective for enhancing the alignment of MXene flakes in fibers and increasing the fiber density. A careful analysis of post-spinning fiber drawing under various temperatures could help maximize the MXene flakes alignment in fibers and further enhance the performance of MXene fibers. For textile processing and wearable applications, it is necessary to achieve MXene fibers with mechanical properties which are comparable to conventional clothing fibers and yarns, such as cotton (tensile strength 250-800 MPa and elongation at break 7%-8%). Other properties of textile fibers such as washability, breathability, and handle (feel of fabric) must also be considered if MXene fibers are to enter practical wearable applications. These suggest the need for the development of innovative fiber spinning strategies to produce MXene fibers that meet the properties requirements of clothing fibers.

To date, the neat MXene fibers have only been used in limited applications, even though they exhibited outstanding properties. In addition to the wearable energy storage and heating applications demonstrated in this review, MXene fibers hold potential for many other wearable applications such as sensing, energy harvesting, antenna, electromagnetic interference shielding, and biomedical applications (*i.e.*, brain electrodes, tissue engineering, wound dressing, and drug delivery). In this respect, the ability to design highly tailored MXene fibers with highly controlled properties and geometries will be critical for meeting the specific requirements of target applications.

Declaration of competing interest

The authors declare that they have no known competing financial interests or personal relationships that could have appeared to influence the work reported in this paper.

Acknowledgments

The authors acknowledge financial support from the National Natural Science Foundation of China (No. 22105106), the Natural Science Foundation of Jiangsu Province of China (No. BK20210603), Nanjing Science and Technology Innovation Project for overseas Students, Start-up Funding from NUPTSF (No. NY221003), and Research Grant from the Royal Society, UK (No. RGS\R1\221044).

References

[1] J. Mu, M.J.D. Andrade, S. Fang, et al., Science 365 (2019) 150–155.
[2] W. Yang, W. Gong, C. Hou, et al., Nat. Commun. 10 (2019) 5541.
[3] M. Liao, C. Wang, Y. Hong, et al., Nat. Nanotechnol. 17 (2022) 372–377.
[4] X. Shi, Y. Zuo, P. Zhai, et al., Nature 591 (2021) 240–245.
[5] J.S. Heo, J. Eom, Y.H. Kim, S.K. Park, Small 14 (2018) 1703034.
[6] K. Jost, G. Dion, Y. Gogotsi, J. Mater. Chem. A 2 (2014) 10776–10787.
[7] T. Zhai, S. Sun, X. Liu, et al., Adv. Mater. 30 (2018) 1706640.

[8] F. Meng, W. Lu, Q. Li, et al., Adv. Mater. 27 (2015) 5113–5131.
[9] C. Müller, L. Ouyang, A. Lund, K. Moth-Poulsen, M.M. Hamedi, Adv. Mater. 31 (2019) 1807286.
[10] S. Seyedin, T. Carey, A. Arbab, et al., Nanoscale 13 (2021) 12818–12847.
[11] S. Sun, B. Liu, H. Zhang, et al., Adv. Energy Mater. 11 (2021) 2003599.
[12] S. Seyedin, P. Zhang, M. Naebe, et al., Mater. Horiz. 6 (2019) 219–249.
[13] W. Weng, P. Chen, S. He, X. Sun, H. Peng, Angew. Chem. Int. Ed. 55 (2016) 6140–6169.
[14] A.K. Yetisen, H. Qu, A. Manbachi, et al., ACS Nano 10 (2016) 3042–3068.
[15] S. Sun, D. Rao, T. Zhai, et al., Adv. Mater. 32 (2020) 2005344.
[16] D. Yu, Q. Qian, L. Wei, et al., Chem. Soc. Rev. 44 (2015) 647–662.
[17] J. Zhang, S. Seyedin, Z. Gu, et al., Part. Part. Syst. Char. 34 (2017) 1600396.
[18] B. Liu, S. Sun, R. Jia, et al., Adv. Funct. Mater. 30 (2020) 1909546.
[19] Smart Fabrics Market Size, Share, and Trends Analysis Report, Grand View Research, Report ID: 978-1-68038-061-3, 2019.
[20] G.G. Wallace, P.R. Teasdale, G.M. Spinks, L.A. Kane-Maguire, Conductive Electroactive Polymers: Intelligent Polymer Systems, CRC press, Boca Raton, 2008.
[21] Z. Zhang, M. Liao, H. Lou, et al., Adv. Mater. 30 (2018) 1704261.
[22] G.A. Snook, P. Kao, A.S. Best, J. Power Sources 196 (2011) 1–12.
[23] P.J. Harris, P.J.F. Harris, Carbon Nanotube Science: Synthesis, Properties and Applications, Cambridge University Press, England, 2009.
[24] R.H. Baughman, A.A. Zakhidov, W.A. De Heer, Science 297 (2002) 787–792.
[25] B. Wiley, Y. Sun, B. Mayers, Y. Xia, Chem. Eur. J. 11 (2005) 454–463.
[26] V.K. Sharma, R.A. Yngard, Y. Lin, Adv. Colloid Interfac. 145 (2009) 83–96.
[27] M. Xu, T. Liang, M. Shi, H. Chen, Chem. Rev. 113 (2013) 3766–3798.
[28] S.Z. Butler, S.M. Hollen, L. Cao, et al., ACS Nano 7 (2013) 2898–2926.
[29] G.R. Bhimanapati, Z. Lin, V. Meunier, et al., ACS Nano 9 (2015) 11509–11539.
[30] B. Anasori, M.R. Lukatskaya, Y. Gogotsi, Nat. Rev. Mater. 2 (2017) 16098.
[31] J. Li, J. Chen, H. Wang, X. Xiao, ChemElectroChem 8 (2021) 648–655.
[32] J. Li, Y. Zhuang, J. Chen, et al., EnergyChem 3 (2021) 100060.
[33] A.K. Geim, K.S. Novoselov, Nat. Mater. 6 (2007) 183–191.
[34] V. Singh, D. Joung, L. Zhai, et al., Prog. Mater. Sci. 56 (2011) 1178–1271.
[35] M. Naguib, M. Kurtoglu, V. Presser, et al., Adv. Mater. 23 (2011) 4248–4253.
[36] Q. Zhao, Y. Jiang, Z. Duan, et al., Chem. Eng. J. 438 (2022) 135588.
[37] H. Huang, J. Zha, S. Li, C. Tan, Chin. Chem. Lett. 33 (2021) 163–176.
[38] T. Qin, Z. Wang, Y. Wang, et al., Nano-Micro Lett. 13 (2021) 183.
[39] M. Naguib, O. Mashtalir, J. Carle, et al., ACS Nano 6 (2012) 1322–1331.
[40] M.R. Lukatskaya, O. Mashtalir, C.E. Ren, et al., Science 341 (2013) 1502–1505.
[41] Z. Ling, C.E. Ren, M.Q. Zhao, et al., P. Natl. Acad. Sci. U. S. A. 111 (2014) 16676–16681.
[42] J. Zhang, N. Kong, S. Uzun, et al., Adv. Mater. 32 (2020) 2001093.
[43] M.R. Lukatskaya, S. Kota, Z. Lin, et al., Nat. Energy 2 (2017) 17105.
[44] M. Hu, Z. Li, G. Li, et al., Adv. Mater. Technol. 2 (2017) 1700143.
[45] J. Zhang, S. Seyedin, Z. Gu, et al., Nanoscale 9 (2017) 18604–18608.
[46] S. Qin, K.A.S. Usman, D. Hegh, et al., ACS Appl. Mater. Interfaces 13 (2021) 36655–36669.
[47] S. Seyedin, E.R.S. Yanza, J.M. Razal, J. Mater. Chem. A 5 (2017) 24076–24082.
[48] Z. Wang, S. Qin, S. Seyedin, et al., Small 14 (2018) 1802225.
[49] J. Zhang, S. Seyedin, S. Qin, et al., Small 15 (2019) 1804732.
[50] S. Seyedin, J. Zhang, K.A.S. Usman, et al., Glob. Chall. 3 (2019) 1900037.
[51] S. Uzun, S. Seyedin, A.L. Stoltzfus, et al., Adv. Funct. Mater. 29 (2019) 1905015.
[52] S. Seyedin, S. Uzun, A. Levitt, et al., Adv. Funct. Mater. 30 (2020) 1910504.
[53] J. Zhang, S. Uzun, S. Seyedin, et al., ACS Central Sci. 6 (2020) 254–265.
[54] A. Levitt, S. Seyedin, J. Zhang, et al., Small 16 (2020) 2002158.
[55] Q. Yang, Z. Xu, B. Fang, et al., J. Mater. Chem. A 5 (2017) 22113–22119.
[56] J. Zhang, S. Seyedin, S. Qin, et al., J. Mater. Chem. A 7 (2019) 6401–6410.
[57] Y. Xia, T.S. Mathis, M.Q. Zhao, et al., Nature 557 (2018) 409–412.
[58] K. Maleski, V.N. Mochalin, Y. Gogotsi, Chem. Mater. 29 (2017) 1632–1640.
[59] R. Liu, J. Li, M. Li, Q. Zhang, H. Wang, ACS Appl. Mater. Interfaces 12 (2020) 46446–46454.
[60] J. Li, N. Kurra, M. Seredych, X. Meng, Y. Gogotsi, Nano Energy 56 (2018) 151–159.
[61] L. Onsager, Ann. NY. Acad. Sci. 51 (1949) 627–659.
[62] W. Eom, H. Shin, R.B. Ambade, et al., Nat. Commun. 11 (2020) 2825.
[63] B. Fang, D. Chang, Z. Xu, C. Gao, Adv. Mater. 32 (2020) 1902664.
[64] Z. Xu, H. Sun, X. Zhao, C. Gao, Adv. Mater. 25 (2013) 188–193.
[65] Y. Deng, T. Shang, Z. Wu, et al., Adv. Mater. 31 (2019) 1802880.
[66] Y. Li, X. Zhang, Adv. Funct. Mater. 32 (2022) 2107767.
[67] H. Shin, W. Eom, K.H. Lee, et al., ACS Nano 15 (2021) 3320–3329.
[68] Q. Zhao, Q. Zhu, J. Miao, et al., Small 15 (2019) 1904293.
[69] X. Wang, Q. Fu, J. Wen, et al., Nanoscale 10 (2018) 20828–20835.
[70] Y. Tian, C. Yang, W. Que, et al., J. Power Sources 369 (2017) 78–86.
[71] S. Li, Z. Fan, G. Wu, et al., ACS Nano 15 (2021) 7821–7832.
[72] Y. Shao, M.F. El-Kady, C.W. Lin, et al., Adv. Mater. 28 (2016) 6719–6726.
[73] A. Borrás, G. Gonçalves, G. Marbán, et al., Chem. Eur. J. 24 (2018) 15903–15911.
[74] Z. Li, T. Huang, W. Gao, et al., ACS Nano 11 (2017) 11056–11065.
[75] Y. Liang, F. Zhao, Z. Cheng, et al., Nano Energy 32 (2017) 329–335.
[76] K. Wang, C.L. Frewin, D. Esrafilzadeh, et al., Adv. Mater. 31 (2019) 1805867.
[77] G. Wu, P. Tan, X. Wu, et al., Adv. Funct. Mater. 27 (2017) 1702493.
[78] X. Zhao, B. Zheng, T. Huang, C. Gao, Nanoscale 7 (2015) 9399–9404.
[79] G. Huang, C. Hou, Y. Shao, et al., Sci. Rep. 4 (2014) 4248.
[80] G. Huang, C. Hou, Y. Shao, et al., Nano Energy 12 (2015) 26–32.
[81] C. Lu, J. Meng, J. Zhang, et al., ACS Appl. Mater. Interfaces 11 (2019) 25205–25217.
[82] X. Chen, J. Jiang, G. Yang, C. Li, Y. Li, Nanoscale 12 (2020) 21325–21333.
[83] S.H. Lee, W. Eom, H. Shin, et al., ACS Appl. Mater. Interfaces 12 (2020) 10434–10442.
[84] H. Li, F. Shao, X. Wen, et al., Electrochim. Acta 371 (2021) 137838.
[85] B. Cheng, P. Wu, ACS Nano 15 (2021) 8676–8685.
[86] Y. Liu, J. Yu, D. Guo, Z. Li, Y. Su, J. Alloy. Compd. 815 (2020) 152403.
[87] J.W. Park, D.Y. Lee, H. Kim, et al., MRS Commun 9 (2019) 114–121.
[88] Z. Wang, Y. Chen, M. Yao, et al., J. Power Sources 448 (2020) 227398.
[89] A. Lipatov, H. Lu, M. Alhabeb, et al., Sci. Adv. 4 (2018) eaat0491.
[90] K. Li, X. Wang, S. Li, et al., Small 16 (2020) 1906851.
[91] Y. Cao, Y. Guo, Z. Chen, et al., Nano Energy 92 (2022) 106689.
[92] J. Li, X. Wang, W. Sun, et al., ChemElectroChem 8 (2021) 151–156.
[93] J. Li, H. Wang, X. Xiao, Energy Environ. Mater. 3 (2020) 306–322.